

Rapid Parameter Estimation for Merging Massive Black Hole Binaries Using ODE-Based Generative Models

Bo Liang^{1 2 3 4}, Minghui Du^{*1}, He Wang^{*4 6}, Yuxiang Xu^{1 2 3 4},
Chang Liu⁷, Xiaotong Wei¹, Peng Xu^{1 2 4 5}, Li-e Qiang⁷, Ziren
Luo^{1 2 4 6}

1 Center for Gravitational Wave Experiment, National Microgravity Laboratory,
Institute of Mechanics, Chinese Academy of Sciences, Beijing 100190, China

2 Key Laboratory of Gravitational Wave Precision Measurement of Zhejiang
Province, Hangzhou Institute for Advanced Study, UCAS, Hangzhou 310024, China

3 Shanghai Institute of Optics and Fine Mechanics, Chinese Academy of Sciences,
Shanghai 201800, China

4 Taiji Laboratory for Gravitational Wave Universe (Beijing/Hangzhou), University
of Chinese Academy of Sciences (UCAS), Beijing 100049, China

5 Lanzhou Center of Theoretical Physics, Lanzhou University, Lanzhou 730000, China

6 International Centre for Theoretical Physics Asia-Pacific (ICTP-AP), University of
Chinese Academy of Sciences (UCAS), Beijing 100049, China

7 National Space Science Center, Chinese Academy of Sciences, Beijing 100190, China

E-mail: hewang@ucas.ac.cn, duminghui@imech.ac.cn

Abstract. Detecting the coalescences of massive black hole binaries (MBHBs) is one of the primary targets for space-based gravitational wave observatories such as LISA, Taiji, and Tianqin. The fast and accurate parameter estimation of merging MBHBs is of great significance for both astrophysics and the global fitting of all resolvable sources. However, such analyses entail significant computational costs. To address these challenges, inspired by the latest progress in generative models, we proposed a novel artificial intelligence (AI) based parameter estimation method called Variance Preserving Flow Matching Posterior Estimation (VPFMPE). Specifically, we utilize triangular interpolation to maintain variance over time, thereby constructing a transport path for training continuous normalization flows. Compared to the simple linear interpolation method used in flow matching to construct the optimal transport path, our approach better captures continuous temporal variations, making it more suitable for the parameter estimation of MBHBs. We also constructed a novel network architecture for gravitational wave feature extraction that outperforms existing methods in terms of training speed and accuracy. Additionally, we creatively introduce a parameter transformation method based on the symmetry in the detector's response function. This transformation is integrated within VPFMPE, allowing us to train the model using a simplified dataset, and then perform parameter estimation on more general data, hence also acting as a crucial factor in improving the training speed. In conclusion, for the first time, within a comprehensive and reasonable parameter range, we have achieved a complete and unbiased 11-dimensional rapid inference for MBHBs in the presence of astrophysical confusion noise using ODE-based generative

models. In the experiments based on simulated data, our model produces posterior distributions comparable to those obtained by nested sampling.

1. Introduction

Gravitational wave (GW) astronomy has made significant progress due to the breakthroughs in ground-based detections led by the LIGO-Virgo-KAGRA network [1, 2, 3]. Scheduled in the upcoming decade, space-based detectors such as the Laser Interferometer Space Antenna (LISA) [4, 5], Taiji [6, 7, 8], and Tianqin [9, 10] aim to detect GWs in the 0.1 mHz - 1 Hz frequency band associated with enormous astrophysical and cosmological sources [11]. As one of the representative projects, Taiji consists of a triangle of three spacecraft (S/Cs) with a baseline separation of 3 million kilometers and aims to detect low-frequency GWs emitted by sources such as compact galactic binaries (GBs) [12], massive black hole binaries (MBHBs) [13], extreme mass ratio inspirals (EMRIs) [14], as well as the stochastic gravitational wave background of astrophysical or cosmological origins.

The merger of MBHB with component masses $10^4 \sim 10^7 M_\odot$ is one of the primary observation targets of space-based GW detectors, since they may shed light upon the growth and merger history of massive black holes, the dynamic behavior of curved spacetime, and the nature of gravity, etc. Due to the presence of the surrounding gas environment, MBHBs may produce detectable electromagnetic (EM) signals in addition to GWs before, during, and after the mergers [15, 16, 17, 18]. Joint EM and GW observation of the same source may unveil the mystery of the evolution of MBHBs and their host galaxies, and provide a new measurement of the cosmic expansion rate, hence shedding light upon the Hubble tension problem in cosmology [19, 20]. For these purposes, it is crucial that the estimation of MBHB parameters, especially the sky location (ecliptic longitude, latitude), should be conducted with high precision and low latency, to guide the search of EM observatories.

Besides, the parameter estimation of merging MBHB must also be robust against the contamination of the confusion foreground formed by tens of millions of Galactic binaries. Indeed, in the area of space-based GW detection, data processing faces the challenge caused by the presence of a large number of astrophysical sources in the measurement band [21]. The non-trivial overlap of individual signals in the time and frequency domains increases the complexity of the task. The accurate analysis of up to $\mathcal{O}(10^4)$ overlapping sources in the data requires the use of global fit techniques [22, 23, 24], namely jointly fitting all sources and noise in the data, which imposes a high challenge on both computational time and resources. The prototype global fit pipeline proposed by Ref. [24] currently requires as many as $\mathcal{O}(10^3)$ CPUs and several days to process the 12-month Lisa Data Challenge (LDC) data, and the issue of computational resources would become even more critical for the multi-year datasets in

the future. Due to these challenges and problems, the aim of this paper is to develop an accelerated and robust method to estimate the parameters of merging MBHBs.

When discussing the efficiency and speed of parameter estimation, the advancement in machine learning technology is revolutionizing our understanding of this area. Currently, most machine learning methods applied to the merging of MBHB use neural posterior estimation(NPE) [25, 26, 27] of discrete normalized flows. NPE has been widely used in fields such as atmospheric retrievals (AR) [28] and ground-based gravitational wave parameters estimation [29, 30]. NPE was also used by the winning entry to the 2023 edition of the ARIEL data challenge [31].

The mission lifetimes of LISA, Taiji, and Tianqin are planned to last for years, during which the payloads, orbits, and noise characteristics will vary over time. Accordingly, the models used for parameter estimation may also need to be regularly updated. As a result, the training speed of the model will be linked to the timeliness of scientific output. However, a significant challenge to the current NPE model in MBHB inference is the extensive training duration, which hampers its ability to conduct real-time data analysis. Additionally, previous research [32] in this area shows that NPE falls short in accurately reproducing the posterior distribution obtained by the benchmark Nested Sampling method. This prolonged training period not only delays the application of the model but also limits its scientific utility in rapidly evolving research contexts. To address these challenges, we applied the latest generative model to MBHBs and made further improvements and optimizations to better solve the problem. Compared to NPE, Flow Matching Posterior Estimation (FMPE) offers more flexibility in designing non-diffusion paths, such as optimal transport paths, and enables direct access to density functions [33]. Moreover, this method can achieve faster and more accurate results than NPE. Nevertheless, FMPE relies solely on simple linear interpolants when constructing optimal transport paths. This reliance impacts the extraction and modeling of MBHB waveform features, which in turn affects the efficiency and accuracy of parameter estimation.

Therefore, to capture the continuous temporal variations and enhance the parameter estimation of MBHBs, we aim to explore more effective methods for constructing transport paths and MBHB wave source feature extraction, which are particularly beneficial and targeted for extracting the continuous waveform characteristics of MBHBs. We consider utilizing trig interpolants to design transport paths [34, 35] that allow for the continuous evolution of MBHB waveform features along the time axis for modeling. This modeling accurately bridges any two probability density functions within a finite time, which belongs to a broad category of continuous-time stochastic processes. We call this method Variance Preserving Flow Matching Posterior Estimation (VPFMPE). Compared to standard Monte Carlo methods, the VPFMPE model achieves comparable performance.

The challenges of parameter estimation for MBHBs not only involve the need for sophisticated algorithms capable of advanced feature extraction and inference, but also lie in the excessively wide prior range of parameters and the resulting complexity of data.

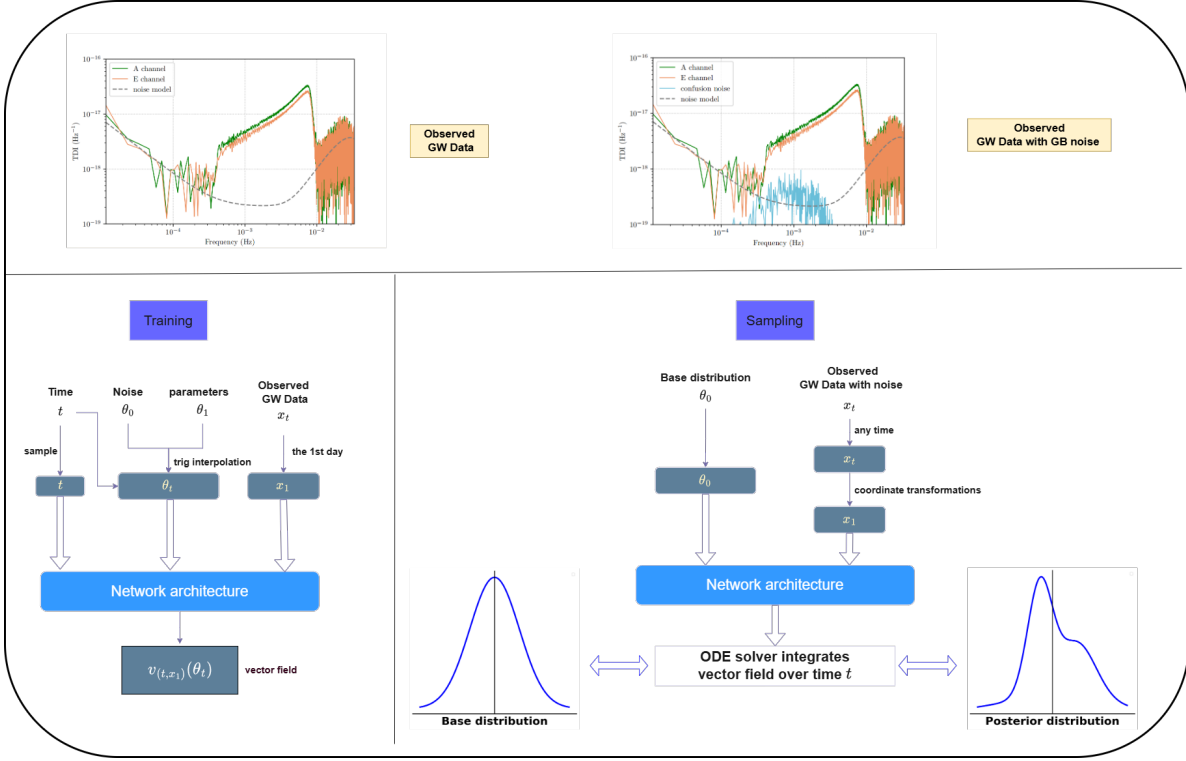


Figure 1: The Diagrams for the training and sampling phases of our model. On the lower left, the training phase is displayed, where t denotes time and x_1 represents the data from the first day of observed MBHBs. In this phase, a feature extractor, as detailed in section 3.1, processes the data to produce a final vector field. This vector field enables the network architecture to learn a transformation from a base distribution (θ_0 , sampled from a Gaussian distribution) to a posterior distribution (θ_1 , sampled from the posterior distribution). On the lower right, the sampling phase is shown. Here, the data with noise (x_t), which includes both confusion noise and instrumental noise from MBHB observations at any time, is mapped back to the first day’s data x_1 using the coordinate transformation described in section 3.2. The Gaussian distribution is then converted into a posterior distribution by solving the ordinary differential equation (ODE) with the vector field learned during the training phase. The top of the image displays simulation data from both the training and sampling phases.

Recent studies [36, 32] adopted priors that do not fully cover the complete physical ranges of parameters. This compromise was due to that setting broad prior ranges during model training can reduce the effectiveness of the model. This underscores the importance of finding a careful balance between the breadth of prior ranges and the accuracy of estimation. To date, no research has managed to achieve unbiased parameter estimation across the entire range of physical priors. Our method is proven to overcome this limitation. In this paper, we expanded the prior ranges of parameters to improve the applicability model.

In order to further enhance the efficiency and effectiveness of model training, we tackled a common complexity faced by space-based gravitational wave detectors, namely the time-varying response function. Utilizing the coordinate transformation of parameters, we can essentially conduct both the model training and the parameter estimation in a coordinate frame fixed to the detector, in which the response function is time-invariant. This strategy significantly simplifies the training task. Consequently, the integration of coordinate transformation and advanced generative models enhances

the speed and accuracy of parameter estimation for MBHBs across an extensive range of priors.

In addition, we have developed a novel network architecture for gravitational wave feature extraction. This architecture illustrated in Figure 4, named TResMlp, introduces the innovation of encoding time t , resulting in superior training speed and accuracy compared to existing methods [33, 32, 36].

The training of the model can be finished in about two days, as shown in Figure 1, which is roughly three times faster than the training duration in our previous work [32]. Additionally, its performance on space-based gravitational wave data is on par with that of traditional Monte Carlo methods. This demonstrates the significant potential of integrating artificial intelligence with VPFMPE techniques to achieve results that are comparable to those obtained with standard Monte Carlo methods.

2. Data Generation and Preprocessing

In this section, we briefly describe the simulation of data used in model training and validation. The IMRPhenomD model is adopted to describe the source-frame waveforms of MBHBs. Given the widely recognized necessity of using Time Delay Interferometry (TDI) to suppress laser frequency noise, Taiji’s response to the MBHB signals is calculated in the form of two noise-orthogonal TDI channels (A, E). Specifically, the fast Fourier domain transfer function derived by Ref. [37] is employed to project the IMRPhenomD waveform to the (A, E) channels, which can be written in a concise form as

$$\tilde{A}(f) = \sum_{\alpha} \mathcal{T}_{\alpha}^A(f, t_f) \tilde{h}_{\alpha}(f), \quad \tilde{E}(f) = \sum_{\alpha} \mathcal{T}_{\alpha}^E(f, t_f) \tilde{h}_{\alpha}(f), \quad \alpha \in \{+, \times\}. \quad (1)$$

As can be seen, the transfer function has a close dependence on the orbits of the detector (through the t_f term). For the sake of speed and simplicity, the motions of Taiji’s satellites are modeled based on an equal-arm analytic orbit with nominal arm-length $L = 3 \times 10^9 \text{m}$ and an orbital period of 1 year.

The TDI response of each MBHB signal can be fully specified by 11 parameters: the chirp mass \mathcal{M}_c , mass ratio $q \equiv m_2/m_1$, the dimensionless spins along the z -axis χ_{z1} and χ_{z2} , the time t_c and phase φ_c at coalescence, the luminosity distance d_L , the inclination angle ι , polarization angle ψ , and the ecliptic coordinate $\{\lambda, \beta\}$, being the longitude and latitude respectively. The priors on these parameters are listed in Table 1. Similar to the LDC-sangria data, the prior range of \mathcal{M}_c covers an order of magnitude. In our previous work [32], considering the complexity of data, we limited the prior ranges of spins to positive values. On this simplified parameter estimation task, NPE has been demonstrated to achieve unbiased estimations. However, its performance is subpar when applied to MBHB data with a complete spin prior. An advantage of the models proposed in this paper is that they are applicable to the complete physical prior range of spins (i.e. $[-1, 1]$). Parameter t_c is defined relative to a reference time t_{ref} . Since the mergers of MBHBs manifest as prominent peaks in the time domain, we

consider a prior range of ~ 2000 s (~ 0.02 day) around t_{ref} . Notably, to simplify the dataset and reduce the difficulty of training, t_{ref} is fixed to the 1th day in the training set. The response function varies with the motion of detectors with a 1-year period, thus a training set with $t_c \in 1 \pm 0.01$ day is far from being sufficient to cover all the observable MBHBs. While, thanks to the method described in Sec. 3.2, our model can be generalized to make inferences throughout the entire task cycle. Besides, the range of d_L corresponds to the redshift range of $z \in [1, 10]$, which is sufficient to encompass the majority of MBHBs observable by space-based GW detectors. The angles ι and β are uniformly distributed in terms of $\cos \iota$ and $\sin \beta$ to represent that the sources are isotropically distributed on the sphere.

Table 1: The prior ranges of parameters. The last column is the alias of parameters used in the code as well as the corner plot.

Parameter	Description	Prior Lower Bound	Prior Upper Bound	Alias in Code
\mathcal{M}_c	Chirp mass of the binary system	$1.0 \times 10^6 M_\odot$	$1.0 \times 10^6 M_\odot$	chirp_mass
q	Ratio of masses of the two black holes	0.1	1.0	mass_ratio
χ_{z1}	Spin of the 1st black hole along the z -axis	-1	1	spin_1
χ_{z2}	Spin of the 2nd black hole along the z -axis	-1	1	spin_2
t_c	-0.01 Time of coalescence relative to the reference time \ddagger , t_{ref}	day	0.01 day	coalescence_time
φ_c	Phase at the moment of coalescence	0 rad	2π rad	coalescence_phase
d_L	Luminosity distance to the binary system	6000 Mpc	100000 Mpc	luminosity_distance
ι	Angle of inclination of the binary orbit	0 rad	π rad	inclination
β	Ecliptic latitude of the binary system	$-\frac{\pi}{2}$ rad	$\frac{\pi}{2}$ rad	latitude
λ	Ecliptic longitude of the binary system	0 rad	2π rad	longitude
ψ	Polarization angle of the gravitational wave	0 rad	π rad	psi

The majority of MBHB’s signal-to-noise ratio(SNR) is contributed by a short duration including the merger phase (typically several hours) [38]. To reasonably avoid the potential overlap of other signals, the time duration for each sample is set to one day, with the merger positioned towards the end of this window. Furthermore, the sampling frequency is set as 1/15 Hz, indicating a Nyquist frequency of 0.033 Hz. This frequency exceeds the highest instantaneous frequency of the waveforms, ensuring comprehensive capture of the signal. Along with the detector responses, we also need the PSD of the noise in each channel. For instrumental noises, according to the current design of the Taiji mission, the one-sided ASDs of the two top-level instrumental noises, namely optical measurement system noise and test mass acceleration noise, are [39]

$$\sqrt{S_{\text{OMS}}(f)} = 8 \times 10^{-12} \sqrt{1 + \left(\frac{2\text{mHz}}{f}\right)^4} \frac{\text{m}}{\sqrt{\text{Hz}}}, \quad (2)$$

$$\sqrt{S_{\text{ACC}}(f)} = 3 \times 10^{-15} \sqrt{1 + \left(\frac{0.4\text{mHz}}{f}\right)^2} \sqrt{1 + \left(\frac{f}{8\text{mHz}}\right)^4} \frac{\text{m/s}^2}{\sqrt{\text{Hz}}}, \quad (3)$$

The total instrumental noise PSDs of the A, E channels $S_n^{A,E}(f)$ are the combinations of these two components (see Ref. [40, 41, 42] for their specific forms). For simplicity, we treat $S_n(f)$ as constant over the whole mission duration. Our training data is a combination of “clean” TDI responses and stationary instrumental noises. On a more realistic ground, the long-term variations and short-term jitters of instrumental noise, along with the typical anomalies such as glitches and gaps should be considered in future work.

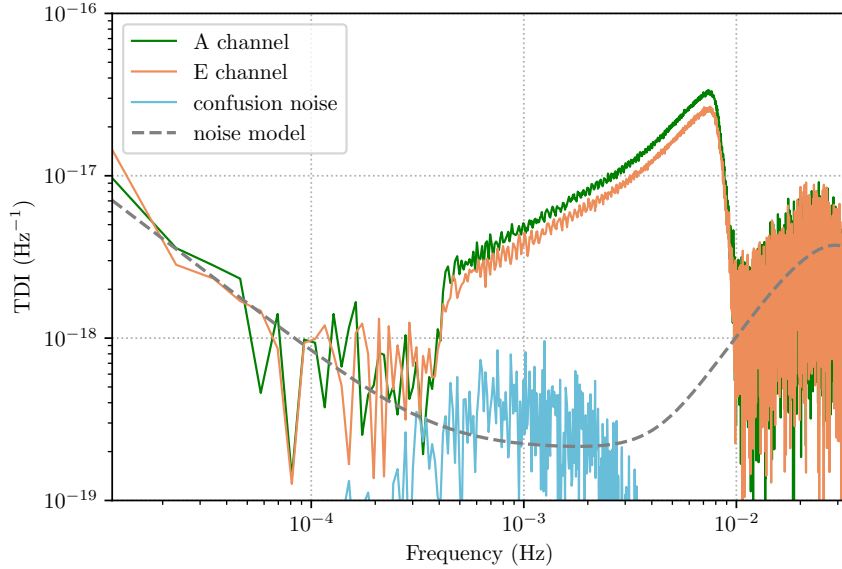


Figure 2: A representative data in the test set. The orange and green curves represent the Fourier transforms of the TDI-A, E data streams, which include GW signals, instrumental noises, and confusion noise. To clearly illustrate the relative strengths of the signal and noises, the blue curve depicts the Fourier transform of the confusion noise, while the gray dashed curve indicates the theoretical amplitude of the instrumental noises.

To test the robustness and generalizability of the model, during the inference stage, we consider a non-stationary noise caused by the unresolvable foreground originating from the overlapping GWs of GBs. This confusion noise is generated with the `FastGB` algorithm [43] from a catalog of $\sim 3 \times 10^7$ GBs provided by the LDC dataset, from which $\sim 2 \times 10^4$ bright sources with SNR greater than 7 were subtracted. This choice of SNR threshold follows the convention of [44, 45, 46, 47]. Shown in Figure 2 is representative data in the test set, including GW signal, instrumental noises, and confusion noise.

3. Methodological Framework

The application of machine learning techniques in the field of gravitational waves has seen widespread success and remarkable achievements [48, 49]. Among these techniques, deep learning has demonstrated exceptional prowess, especially in processing ground-based gravitational wave data [50, 51, 52, 53, 54, 55, 56, 57, 58].

NPE with normalizing flows. Neural Posterior Estimation (NPE) combined with Normalizing Flows (NF) is used to directly fit the posterior distribution $p(\theta|x)$. In this approach, an invertible mapping ψ_x transforms the base distribution $p_0(\mathbf{z})$ into the target distribution $q(\theta|x)$:

$$q(\theta|x) = p_0(\psi_x^{-1}(\theta)) \det \left| \left(\frac{\partial \psi_x^{-1}(\theta)}{\partial \theta} \right) \right|. \quad (4)$$

NPE is trained using a maximum likelihood objective and simplifies the expectation using Bayes' theorem.

$$L_{\text{NPE}} = -E_{p(\theta)p(x|\theta)} \log q(\theta|x). \quad (5)$$

Once training is complete, NPE can efficiently perform inference on new observations x and provide exact density evaluations of $q(\theta|x)$. This method retains the expressive power and computational efficiency of normalizing flows while achieving posterior fitting.

Continuous Normalizing Flows for parameter estimation. Continuous Normalizing Flows (CNFs) transform a simple base distribution into a more complex distribution by describing this transformation through continuous time $t \in [0, 1]$. For each t , the flow is defined by a vector field $v_{t,x}$ on the sample space. This vector field represents the trajectory velocity of the samples at any given time t .

$$\frac{d}{dt}\psi_{t,x}(\theta) = v_{t,x}(\psi_{t,x}(\theta)). \quad (6)$$

The conversion between the base distribution (at $t = 0$) and the target distribution (at $t = 1$) is achieved by integration. A straightforward approach to training Continuous Normalizing Flows (CNFs) involves starting with a given base distribution and using an ODE solver to obtain the target distribution. This target distribution is then constrained to match the real data distribution by minimizing a divergence measure, such as the KL divergence.

Because many intermediate trajectories are unknown, inferring the distribution (either through sampling or likelihood computation) requires repeatedly simulating the ODE, leading to a significant computational burden.

However, Flow matching provides alternative training objectives for CNFs, Dax et al. [33] apply flow matching [59] to simulation-based inference. The loss function of FMPE is expressed as:

$$L_{\text{FMPE}} = E_{t \sim p(t), \theta_1 \sim p(\theta), x \sim p(x|\theta_1), \theta_t \sim p_t(\theta_t|\theta_1)} \| v_{t,x}(\theta_t) - u_t(\theta_t|\theta_1) \|^2. \quad (7)$$

Here, $v_{t,x}(\theta_t)$ represents the vector field that generates the path to the target probability distribution, and $u_t(\theta_t|\theta_1)$ is the sample-conditioned vector field. FMPE introduces a Gaussian path with time-dependent means $t\theta_1$ and standard deviations $1 - (1 - \sigma)t$.

$$p_t(\theta|\theta_1) = N(t\theta_1, 1 - (1 - \sigma)t). \quad (8)$$

FMPE defines the sample-conditioned vector field is

$$u_t(\theta|\theta_1) = \frac{\theta_1 - (1 - \sigma)\theta_0}{1 - (1 - \sigma)t}. \quad (9)$$

In our work, we reference the studies by Albergo et al. [34, 35] and utilize triangular interpolation to define the time-dependent mean and standard deviation, thus constructing the Gaussian path and sample-conditioned vector field as follows:

$$p_t(\theta|\theta_1) = N(\sin(\frac{\pi}{2t})\theta_1 + \cos(\frac{\pi}{2t})\theta_0, \sigma). \quad (10)$$

$$u_t(\theta|\theta_1) = \frac{\pi}{2(\cos(\frac{\pi}{2t})\theta_1 - \sin(\frac{\pi}{2t})\theta_0)}. \quad (11)$$

We call this method Variance Preserving Flow Matching Posterior Estimation and use it to train continuous normalization flows. We show the differences between the two methods in Table 2.

Table 2: A table with constructing transport paths differences. FMPE uses linear interpolation to construct transport paths, while VPFMPE uses trig interpolants to construct transport paths.

	Interpolator Method	Mean of the probability path	Standard deviation of the probability path
FMPE	linear	$t\theta_1$	$1 - (1 - \sigma)t$
VPFMPE	trig	$\sin(\frac{\pi}{2t})\theta_1 + \cos(\frac{\pi}{2t})\theta_0$	σ

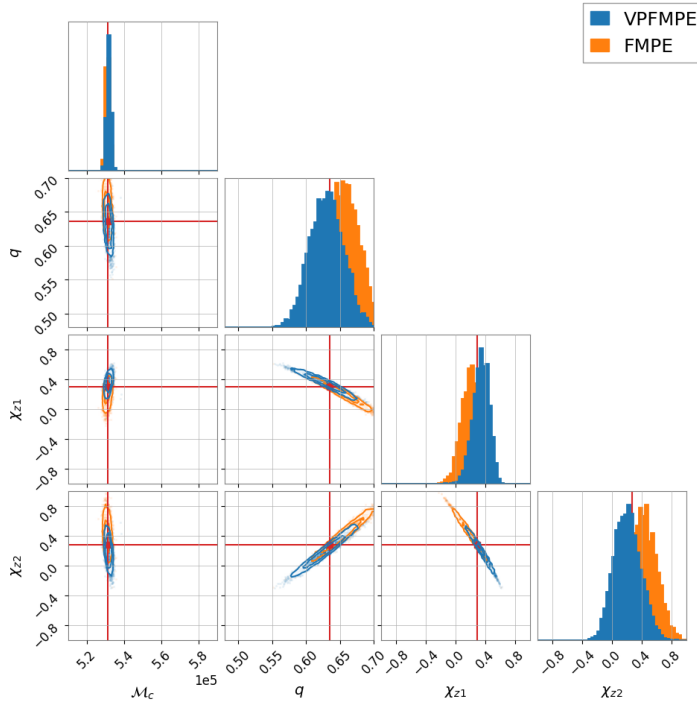


Figure 3: Comparison of the posterior distributions of the two methods. Blue represents the posterior distribution of the VPFMPE method on the injected MBHB signal. Orange represents the posterior distribution of the FMPE method on the injected MBHB signal. The red line represents the true value of the injected MBHB signal.

Comparison of methods. To demonstrate the performance of the transport path constructed by VPFMPE, we randomly injected an MBHB signal and compared the FMPE method with the VPFMPE method. Both models were trained using the same learning rate, optimizer, and gravitational wave feature extractor to ensure fairness. We show in Figure 3 a comparison of the posterior estimates of the four parameters of the injected MBHB signal by the two methods.

Discussion. The NPE network just only one-third allocated to the feature extractor network for GW data. However, the ODE-based generative model only needs

to parameterize a simple vector field, so it can devote its full network capacity to interpreting the higher dimensions [33].

3.1. Network architecture

A key challenge in space-based gravitational wave parameter estimation lies in managing the high-dimensional nature of its data. To address this, it is essential to develop a feature extraction network capable of transforming the high-dimensional input data into a more manageable, low-dimensional representation [29, 32, 60]. This transformation is critical for adjusting the dimensionality of the final feature vector to match that of the parameter vector θ , enabling the network to effectively parameterize the conditional vector field $(t, x, \theta) \rightarrow v_{t,x}(\theta)$ [33]. Achieving accurate parameterization of this conditional vector field is fundamental to the construction of an effective network structure. In recent years, DeResNet networks have been commonly used as the

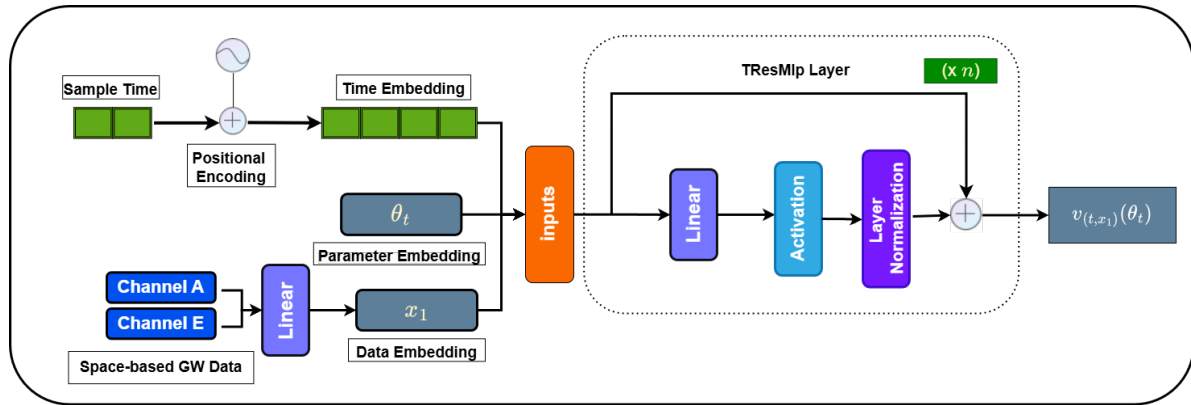


Figure 4: TResMlp Network Architecture: Initially, the frequency vector f is used to encode the position of time t . Sine and cosine functions are then applied to extract periodic features from time t , resulting in the “Time Embedding”. Subsequently, a “Linear” layer maps the two channels of the space-based GW data to produce the “Data Embedding”. Finally, all obtained embeddings are input into a Multi-Layer Perceptron (MLP) with a residual structure to generate the final output $v_{(t,x_1)}(\theta_t)$.

backbone network for feature extraction in ground-based gravitational wave parameter estimations or space-based gravitational wave parameter estimation [57, 32, 33, 53], and Gated Linear Unit(GLU)-conditioning [61] can be optionally used for information aggregation of (θ, t) .

However, if information about the actual parameter θ is not properly handled or retained during the process of aggregating (θ, t) information using GLU, it could potentially lead to a loss of information about θ . To encode the time t more effectively and ensure that our feature extraction network captures its dynamic nature, we introduce a frequency vector f . This frequency vector f adapts dynamically to changes in the parameters of the wave source, allowing for a more precise encoding of time t . To capture the periodic features of time, we employ sine and cosine functions for encoding. Our network architecture, referred to as TResMlp, is shown in Figure 4.

We trained the CNFs of MBHBs using two different network architectures. To ensure fairness, the two models had identical parameters such as the optimizer and

learning rate, differing only in their network structures. Additionally, both architectures used the same hidden layer configuration. We show in Figure 5 a comparison of the posterior estimates of the four parameters of the injected MBHBs signal by the two models.

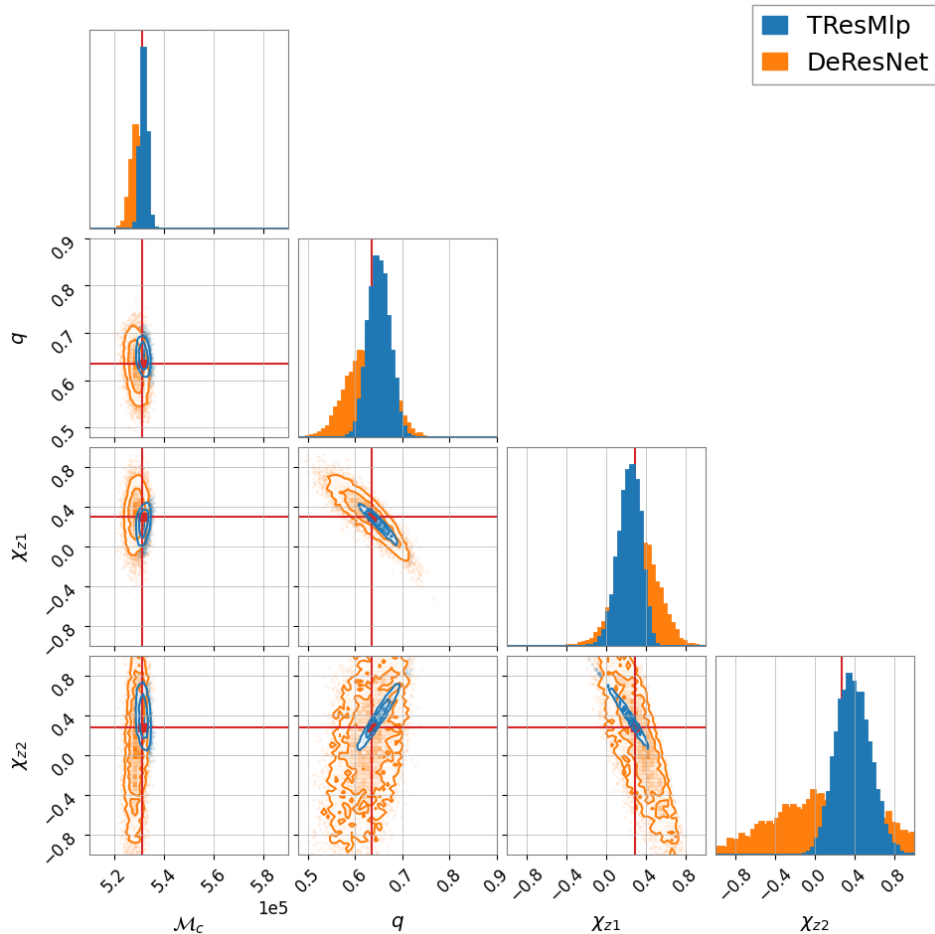


Figure 5: Comparison of the posterior distributions of the two network architectures. The blue represents the posterior distribution plot of CNFs trained using the TResMlp network. The orange represents the posterior distribution plot of CNFs trained using the DeResNet network. The red line represents the true value of the MBHBs.

Compared to the DeResNet model that use GLU-conditioning for aggregating information about (θ, t) [57, 32, 33, 53], our network architecture, TResMlp, demonstrates faster training speed and higher precision with the same hidden layers. More experiments and comparisons of related models are described in detail in Section 4.

3.2. Coordinate Transformation and Model Generalization Strategy

To simplify the dataset and reduce the difficulty of training, the coalescence times of MBHBs are set within 1 ± 0.02 day in the training set (see Sec. 2). While the response function of detector to GW signals varies in time with a one-year period, thus in principle the model trained on this dataset can only be applied to MBHBs that merge

within 1 ± 0.02 day. While, thanks to the generalization strategy in this section, the application scope of the model can be extended to the whole mission lifetime.

In this paper, the time of coalescence (dubbed t_c) is defined relative to a reference time t_{ref} . The complexity of space-based GW data partly lies in the annual modulation of detector response due to the orbital motion of detector constellation around the sun. In other words, the mapping between GW data and MBHB parameters varies with t_{ref} . This significantly increases the complexity of the training set, which would severely damage the training efficiency and the performance of the model. To tackle this challenge, we exploit the symmetry (invariance) of the system, fix the training data around a certain $t_{\text{ref}0}$, and then the trained model is generalized via our transformation rule to make inferences at any time. The idea behind this is a paradigm that combines physical information with neural networks, and methods belonging to this family, such as the group-equivariant neural posterior estimation [62, 60], have shown broad application prospects.

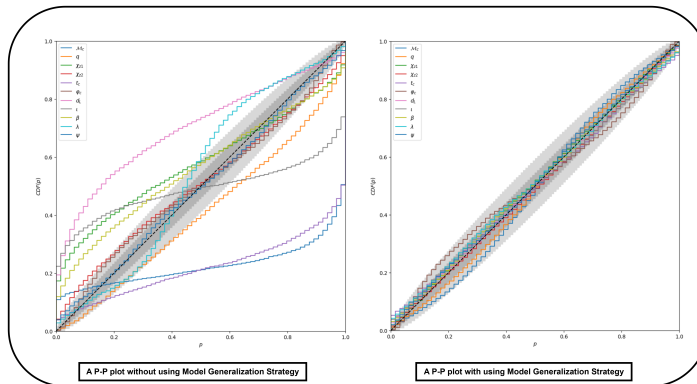


Figure 6: Comparison of the effect of the model generalization strategy on model performance. The left panel shows the P-P plot without the model generalization strategy, while the right panel shows the P-P plot with the model generalization strategy. Both plots are for a set of 4000 injections with added instrument noise and reference times ranging from 1 to 365 days. Ideally, the cumulative distribution function of these percentiles for each parameter should align closely with the diagonal line, indicating optimal network performance. In such a case, the percentiles would be uniformly distributed between 0 and 1. The grey regions on the plot represent the 1σ and 2σ confidence intervals.

We describe the transformation rule as follows. We define two coordinate systems, namely the Solar System Barycenter (SSB), in which physical quantities are indexed with “S”, and the Taiji detector reference frame, in which physical quantities are indexed with “T”. The parameters which vary with the coordinate systems are $\{t_c, \lambda, \beta, \psi\}$, where t_c should be interpreted as the time of arrival at the origin of the coordinate system (relative to t_{ref}). Since the data in consideration last only for one day, for preliminary parameter estimation tasks, the location of MBHB remains stationary relative to the Taiji reference frame, and the mapping between source parameters θ_T and TDI response is independent of t_{ref} . This is precisely the symmetry based on which we can achieve model generalization. The t_{ref} -dependent coordinate transformation from Taiji frame to SSB frame is denoted as $f_{t_{\text{ref}}} : \theta_T \rightarrow \theta_{S,t_{\text{ref}}}$ (see Ref. [63] for the expression of f). The parameters are firstly inferred with the model trained around $t_{\text{ref}0}$, hence dubbed $\theta_{S,t_{\text{ref}0}}$,

and the targeted parameters $\boldsymbol{\theta}_{S,t_{\text{ref}}}$ can be obtained following two steps:

$$\boldsymbol{\theta}_T = f_{t_{\text{ref}0}}^{-1}(\boldsymbol{\theta}_{S,t_{\text{ref}0}}), \quad \boldsymbol{\theta}_{S,t_{\text{ref}}} = f_{t_{\text{ref}}}(\boldsymbol{\theta}_T), \quad (12)$$

or in terms of posterior distributions:

$$p(\boldsymbol{\theta}_{S,t_{\text{ref}}}|d) = p(\boldsymbol{\theta}_{S,t_{\text{ref}0}}|d) J(f_{t_{\text{ref}0}}) J(f_{t_{\text{ref}}}^{-1}), \quad (13)$$

with $J(f_{t_{\text{ref}0}})$ and $J(f_{t_{\text{ref}}}^{-1})$ being the Jacobian determinants corresponding to $f_{t_{\text{ref}0}}$ and $f_{t_{\text{ref}}}^{-1}$, respectively. Formula (13) looks similar to the transformations in normalizing flows, except that the mapping $f_{t_{\text{ref}}}$ is constructed based on our understanding of the system, instead of training a neural network. Training a network to represent this transformation is unnecessary since we possess comprehensive knowledge of its form and can effortlessly compute it. As a result, The embedding of this physical information greatly simplifies training tasks.

Below, we describe how models can be combined with the model generalization strategy. Firstly, during the dataset generation, the merger times of MBHBs are limited to 0.02 days centered at a specific reference time (the 1st day). This significantly simplifies the dataset’s complexity and reduces the challenge of MBHB parameter estimation. Subsequently, we employ VPFMPE as the loss function for training CNFs. We utilize the novel network architecture TResMlp as the gravitational wave feature extractor, labeling this approach as VPFMPE-TResMlp.

In the inference phase, we use the model generalization strategy to map the reference time data for inference to the reference time data fixed during training. This allows the model to be trained on only one day of data but tested and applied to data spanning an entire year. We use the P-P plot in Figure 6 to demonstrate the importance of using a model generalization strategy.

4. Experiments

To ensure unbiased parameter estimation, we examine our algorithm on injected GW signals and noise in this section. For the parameter estimation of the signals, we employed the four models mentioned above: VPFMPE-TResMlp, FMPE-TResMlp, FMPE-DeResNet [33], and NPE-DeResNet [32]. We applied the model generalization strategy 3.2 to all four models by default. Otherwise, due to the complexity of the dataset, the models would lack inference capability.

Table 3: In the 850 simulations, we compared the correlation coefficients between the true values and the recovered values for the four models. In addition, in the last column of the table, we have included the training time for the three models.

	\mathcal{M}_c	q	χ_{z1}	χ_{z2}	d_L	Training time
VPFMPE-TResMlp	0.9978	0.9790	0.9723	0.8163	0.9408	\approx 2.0 days
FMPE-TResMlp	0.9978	0.9787	0.9719	0.8139	0.9400	\approx 2.0 days
FMPE-DeResNet	0.9970	0.9762	0.9563	0.7174	0.9397	\approx 2.3 days
NPE-DeResNet	0.9261	0.8647	0.6620	0.1681	0.8634	\approx 6.5 days

To demonstrate the effectiveness of our algorithm and validate that the recovered probability distribution accurately represents the confidence we should have in the signal parameters, we conducted extensive testing on simulated signals and noise. We injected 850 waveforms drawn from the prior, along with residual instrumental and foreground confusion noise. We will take the median of the recovered values as the point estimate and calculate the correlation coefficient with the true values of the parameters. The correlation coefficient reflects the degree of linear correlation between the true value distribution and the estimated values. A coefficient value of 1 indicates perfect consistency between the estimated and true values. Note that the reference times of these testing signals are randomly distributed throughout the year, rather than being fixed to the 1st day.

Our results are presented in Table 3. In the final column of the Table 3, we have included the approximate training times for the three models. The VPFMPE-TResMlp model achieved the best results and had the fastest training time. For t_c , φ_c , ι , β , λ , and ψ , due to the presence of multimodality (i.e. there is more than one peak in the posterior distributions), using the median as a point estimate is not applicable.

To date, existing research has not yet succeeded in providing unbiased estimates of MBHBs across the entire parameter space. For example, Ref. [36] only focused on four parameters, and Ref. [32] have limited to positive spins. Also, we use machine learning techniques for complete parameter estimation of MBHBs and achieve comparable results to nested sampling. Therefore, in subsequent comparisons, we will only compare the results of VPFMPE-TResMlp to those of the MCMC method.

The aim of our ODE-based generative models for MBHBs is to reproduce the comparable posterior distribution as the MCMC method. Thus, by comparing the results of Bayesian inference on the same event, the performance of the model can be better assessed. In this case, we use Nested Sampling [64, 65, 66] as a Monte Carlo technique for comparison experiments, as shown in Figure 7.

An illustration demonstrating an example using the same prior probabilities outlined in Table 1 is provided in Figure 7, where a test injection is subjected to confusion noise on the 30th reference day. The injected GW signal originates from an MBHB with a total signal-to-noise ratio of 1543, and its parameters are detailed in Table 4. Compared to the standard nested sampling technique, our model exhibited results similar to the traditional nested sampling, demonstrating consistency in the sense of the degeneracy among extrinsic parameters 4. This consistency aligns with the crucial physical characteristics of MBHBs. Note that compared to nested sampling, our machine learning process always produces similar posterior distributions on t_c , d_L , ι , β , λ , and ψ .

We have achieved accurate estimates of the sky position parameters. This is most advantageous since accurate and reliable estimates of the sky position parameters (longitude, latitude) are useful in guiding the search for electromagnetic observatories.

We have collated the true values of the injections alongside the results generated by both the model and the nested sampling process in Table 4. This provides a concise

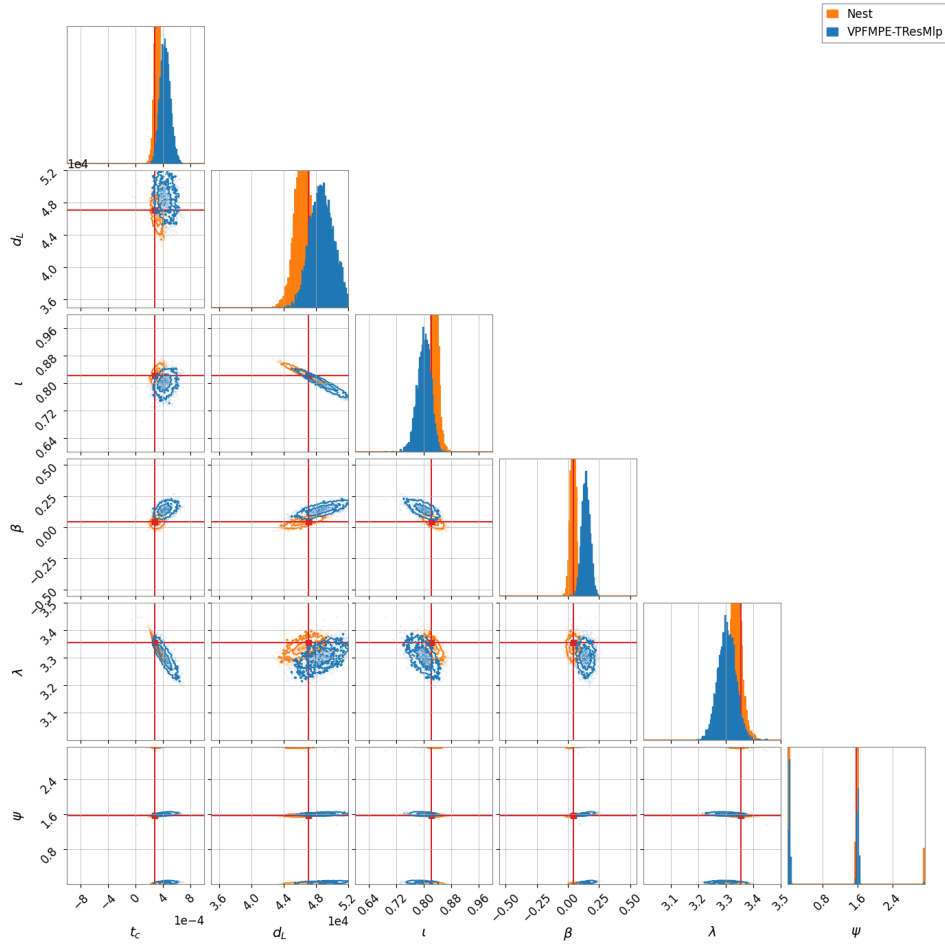


Figure 7: Corner plot of parameter posterior distributions for gravitational wave signals injected with instrumental and confusion noise. The blue contours illustrate the two-dimensional joint posteriors obtained from our (VPFMPE-TResMlp) model, with peaks selected based on t_c that align with true values. In contrast, the orange contours represent the corresponding posteriors obtained from benchmark analysis using Nested Sampling. For each model, the contour boundaries respectively encompass 95% and 60% confidence levels. The true parameter values of the simulated signal are indicated by red vertical and horizontal lines.

overview of the performance of each method.

A noteworthy phenomenon is that our machine learning pipeline produces a posterior similar to the nested sampling approach in terms of extrinsic parameters, and the posterior distributions of both converge in the same order of magnitude.

In the final part of the results, we explore the computational efficiency of the algorithm. Table 5 shows the speed of generating posterior samples using nested sampling compared to the VPFMPE method. It is important to note that we used nested sampling to search near the true intrinsic parameter values of the injected MBHB. In practice, the time consumed by nested sampling is significantly longer than the times listed in the table. Even under these conditions, our VPFMPE method remains two orders of magnitude faster than the nested sampling method.

Our model not only prioritizes efficiency but also generates a posterior distribution similar to nested sampling. Moreover, it is well-suited for the majority of MBHB sources

Table 4: This table compares the parameters injected in the prior with the parameters recovered by the Nested Sampling and VPFMPE-TResMlp methods. The GW signal is emitted by a merging MBHB with a total SNR of 1543. The recovered values are accompanied by their 1σ confidence regions.

Parameter	Injected value	VPFMPE-TResMlp	Nest
$\mathcal{M}_c [M_\odot]$	531067.4	$528444.8000^{+1141.3900}_{-1206.2360}$	$531038.3974^{+125.0852}_{-107.2206}$
q	0.6355	$0.5994^{+0.0236}_{-0.0220}$	$0.6405^{+0.0060}_{-0.0070}$
χ_{z1}	0.2930	$0.4051^{+0.0858}_{-0.1042}$	$0.2636^{+0.0318}_{-0.0259}$
χ_{z2}	0.2726	$0.0273^{+0.1807}_{-0.1552}$	$0.3233^{+0.0409}_{-0.0517}$
t_c [day]	0.00028	$0.0004^{+0.0001}_{-0.0001}$	$0.0003^{+0.0000}_{-0.0000}$
φ_c [rad]	0.5412	$3.1765^{+1.7528}_{-1.8449}$	$3.6714^{+1.6062}_{-3.0978}$
d_L [Mpc]	47054.1	$48698.8670^{+1568.7870}_{-1486.6328}$	$46334.8753^{+882.4137}_{-891.2652}$
ι [rad]	0.8207	$0.8004^{+0.0191}_{-0.0207}$	$0.8298^{+0.0098}_{-0.0109}$
β [rad]	0.0459	$0.1405^{+0.0340}_{-0.0317}$	$0.0401^{+0.0188}_{-0.0188}$
λ [rad]	3.3544	$3.3024^{+0.0317}_{-0.0322}$	$3.3350^{+0.0188}_{-0.0167}$
ψ [rad]	1.5634	$1.5680^{+0.0442}_{-1.5388}$	$1.5692^{+0.0188}_{-1.5613}$

Table 5: Comparison of computational time required by different posterior sampling approaches to generate their respective samples.

	Number of Posterior Samples	Runtime (seconds)	Time per Sample
Nested Sampling	11215	3000	0.26750
VPFMPE	14336	240	0.01674

anticipated by future Taiji observations. This contribution will significantly enhance global fit analysis.

5. Conclusions

In this study, we have demonstrated the inaugural application of ODE-based generative models in the field of space-based GW detection, taking the parameter estimation of merging MBHBs as a representative example. We recommend the use of ODE-based generative models, particularly the VPFMPE method, as the mainstream machine learning inference approach.

Our method provides comprehensive statistical inference for the 11-dimensional parameters of MBHBs, establishing a new benchmark in this area. This approach, as opposed to likelihood-based inference methods, can lead to both faster training and more accurate estimation.

Furthermore, we propose the integration of model generation strategy based on the symmetry of the system with ODE-based generative models. This enables us to simplify the training task, while still obtaining a model that is applicable to the entire mission period. Note that the coordinate transformation and ODE-based generative models are theoretically applicable to other space-based missions such as LISA.

It is also noteworthy that our method exhibits robustness against challenges such as confusion noise and the complexities of varying reference times, highlighting its reliability and potential for broader applications. The significant speed of our method, surpassing traditional techniques by orders of magnitude, positions it as a valuable tool

for preprocessing in global fitting. Moreover, the precise and reliable estimation of sky location parameters (longitude, latitude) proves beneficial in guiding the search for electromagnetic observatories.

This acceleration in data processing and analysis not only streamlines workflows but also broadens the horizons for gravitational wave data exploration. Overall, these advancements herald a transformative era in space-based GW detection, fortifying the capabilities of missions like Taiji and bringing us closer to unraveling the mysteries of the universe.

6. Acknowledgements

This study is supported by the National Key Research and Development Program of China (Grant No. 2021YFC2201901, Grant No. 2021YFC2203004, Grant No. 2020YFC2200100 and Grant No. 2021YFC2201903). International Partnership Program of the Chinese Academy of Sciences, Grant No. 025GJHZ2023106GC.

- [1] The LIGO Scientific Collaboration, J Aasi, et al. Advanced ligo. *Classical and Quantum Gravity*, 32(7):074001, mar 2015.
- [2] Fet al Acernese, M Agathos, K Agatsuma, Damiano Aisa, N Allemandou, Aea Allocca, J Amarni, Pia Astone, G Balestri, G Ballardin, et al. Advanced virgo: a second-generation interferometric gravitational wave detector. *Classical and Quantum Gravity*, 32(2):024001, 2014.
- [3] T. Akutsu et al. Kagra: 2.5 generation interferometric gravitational wave detector. *Nature Astronomy*, 3(1):35–40, 2019.
- [4] Pau Amaro-Seoane, Heather Audley, Stanislav Babak, John Baker, Enrico Barausse, Peter Bender, Emanuele Berti, Pierre Binetruy, Michael Born, Daniele Bortoluzzi, et al. Laser interferometer space antenna, 2017.
- [5] John Baker, Jillian Bellovary, Peter L Bender, Emanuele Berti, Robert Caldwell, Jordan Camp, John W Conklin, Neil Cornish, Curt Cutler, Ryan DeRosa, et al. The laser interferometer space antenna: unveiling the millihertz gravitational wave sky, 2019.
- [6] Wen-Rui Hu and Yue-Liang Wu. The Taiji Program in Space for gravitational wave physics and the nature of gravity. *National Science Review*, 4(5):685–686, 10 2017.
- [7] Ziren Luo, Yan Wang, Yueliang Wu, Wenrui Hu, and Gang Jin. The Taiji program: A concise overview. *Progress of Theoretical and Experimental Physics*, 2021(5):05A108, 07 2020.
- [8] Taiji Scientific Collaboration, Yue-Liang Wu, et al. China’s first step towards probing the expanding universe and the nature of gravity using a space borne gravitational wave antenna. *Communications Physics*, 4(1):34, December 2021.
- [9] Jun Luo, Li-Sheng Chen, Hui-Zong Duan, Yun-Gui Gong, Shoucun Hu, Jianghui Ji, Qi Liu, Jianwei Mei, Vadim Milyukov, Mikhail Sazhin, et al. Tianqin: a space-borne gravitational wave detector. *Classical and Quantum Gravity*, 33(3):035010, jan 2016.
- [10] Jun Luo, Li-Sheng Chen, Hui-Zong Duan, Yun-Gui Gong, Shoucun Hu, Jianghui Ji, Qi Liu, Jianwei Mei, Vadim Milyukov, Mikhail Sazhin, Cheng-Gang Shao, Viktor T Toth, Hai-Bo Tu, Yamin Wang, Yan Wang, Hsien-Chi Yeh, Ming-Sheng Zhan, Yonghe Zhang, Vladimir Zharov, and Ze-Bing Zhou. Tianqin: a space-borne gravitational wave detector. *Classical and Quantum Gravity*, 33(3):035010, jan 2016.
- [11] Gerhard Heinzl, Claus Braxmaier, Roland Schilling, Albrecht Rüdiger, David Robertson, M Te Plate, Vinzenz Wand, K Arai, Ulrich Johann, and Karsten Danzmann. Interferometry for the lisa technology package (ltp) aboard smart-2. *Classical and Quantum Gravity*, 20(10):S153, 2003.
- [12] Xue-Hao Zhang, Shao-Dong Zhao, Soumya D Mohanty, and Yu-Xiao Liu. Resolving galactic

- binaries using a network of space-borne gravitational wave detectors. *Physical Review D*, 106(10):102004, 2022.
- [13] Antoine Klein, Enrico Barausse, Alberto Sesana, Antoine Petiteau, Emanuele Berti, Stanislav Babak, Jonathan Gair, Sofiane Aoudia, Ian Hinder, Frank Ohme, et al. Science with the space-based interferometer elisa: Supermassive black hole binaries. *Physical Review D*, 93(2):024003, 2016.
- [14] Andrea Maselli, Nicola Franchini, Leonardo Gualtieri, and Thomas P Sotiriou. Detecting scalar fields with extreme mass ratio inspirals. *Physical Review Letters*, 125(14):141101, 2020.
- [15] Bence Kocsis, Zsolt Frei, Zoltán Haiman, and Kristen Menou. Finding the electromagnetic counterparts of cosmological standard sirens. *The Astrophysical Journal*, 637(1):27, jan 2006.
- [16] Alessandra De Rosa, Cristian Vignali, Tamara Bogdanović, Pedro R. Capelo, Maria Charisi, Massimo Dotti, Bernd Husemann, Elisabeta Lusso, Lucio Mayer, Zsolt Paragi, Jessie Runnoe, Alberto Sesana, Lisa Steinborn, Stefano Bianchi, Monica Colpi, Luciano del Valle, Sándor Frey, Krisztina É. Gabányi, Margherita Giustini, Matteo Guainazzi, Zoltan Haiman, Noelia Herrera Ruiz, Rubén Herrero-Illana, Kazushi Iwasawa, S. Komossa, Davide Lena, Nora Loiseau, Miguel Perez-Torres, Enrico Piconcelli, and Marta Volonteri. The quest for dual and binary supermassive black holes: A multi-messenger view. *New Astronomy Reviews*, 86:101525, 2019.
- [17] Milos Milosavljevic and E. S. Phinney. The Afterglow of massive black hole coalescence. *Astrophys. J. Lett.*, 622:L93–L96, 2005.
- [18] M. Dotti, R. Salvaterra, A. Sesana, M. Colpi, and F. Haardt. On the search of electromagnetic cosmological counterparts to coalescences of massive black hole binaries. *Monthly Notices of the Royal Astronomical Society*, 372(2):869–875, 09 2006.
- [19] Nicola Tamanini, Chiara Caprini, Enrico Barausse, Alberto Sesana, Antoine Klein, and Antoine Petiteau. Science with the space-based interferometer eLISA. III: Probing the expansion of the Universe using gravitational wave standard sirens. *JCAP*, 04:002, 2016.
- [20] Maria Dainotti, Biagio De Simone, Giovanni Montani, Tiziano Schiavone, and Gaetano Lambiase. The Hubble constant tension: current status and future perspectives through new cosmological probes. *PoS, CORFU2022:235*, 2023.
- [21] Jean-Baptiste Bayle, Béatrice Bonga, Chiara Caprini, Daniela Doneva, Martina Muratore, Antoine Petiteau, Elena Rossi, and Lijing Shao. Overview and progress on the laser interferometer space antenna mission. *Nature Astronomy*, 6(12):1334–1338, 2022.
- [22] Neil J. Cornish and Jeff Crowder. Lisa data analysis using markov chain monte carlo methods. *Phys. Rev. D*, 72:043005, Aug 2005.
- [23] Tyson B. Littenberg, Neil J. Cornish, Kristen Lackeos, and Travis Robson. Global analysis of the gravitational wave signal from galactic binaries. *Phys. Rev. D*, 101:123021, Jun 2020.
- [24] Tyson B. Littenberg and Neil J. Cornish. Prototype global analysis of lisa data with multiple source types. *Phys. Rev. D*, 107:063004, Mar 2023.
- [25] George Papamakarios and Iain Murray. Fast ϵ -free inference of simulation models with bayesian conditional density estimation. In *Neural Information Processing Systems*, 2016.
- [26] Jan-Matthis Lueckmann, Pedro J. Gonçalves, Giacomo Bassetto, Kaan Öcal, Marcel Nonnenmacher, and Jakob H. Macke. Flexible statistical inference for mechanistic models of neural dynamics. In *Neural Information Processing Systems*, 2017.
- [27] David S. Greenberg, Marcel Nonnenmacher, and Jakob H. Macke. Automatic posterior transformation for likelihood-free inference. In *International Conference on Machine Learning*, 2019.
- [28] Timothy D. Gebhard, Jonas Wildberger, Maximilian Dax, Daniel Angerhausen, Sascha P. Quanz, and Bernhard Scholkopf. Inferring atmospheric properties of exoplanets with flow matching and neural importance sampling. *ArXiv*, abs/2312.08295, 2023.
- [29] Maximilian Dax, Stephen R. Green, Jonathan R. Gair, Jakob H. Macke, Alessandra Buonanno, and Bernhard Scholkopf. Real-time gravitational-wave science with neural posterior estimation. *Physical review letters*, 127 24:241103, 2021.

- [30] Stephen R. Green, Christine M. Simpson, and Jonathan R. Gair. Gravitational-wave parameter estimation with autoregressive neural network flows. *ArXiv*, abs/2002.07656, 2020.
- [31] Mayeul Aubin, Carolina Cuesta-Lázaro, Ethan Tregidga, Javier Viana, Cecilia Garraffo, Iouli E. Gordon, Mercedes López-Morales, Robert J. Hargreaves, Vladimir Yu. Makhnev, Jeremy J. Drake, Douglas P. Finkbeiner, and Phillip A. Cargile. Simulation-based inference for exoplanet atmospheric retrieval: Insights from winning the ariel data challenge 2023 using normalizing flows. *ArXiv*, abs/2309.09337, 2023.
- [32] Minghui Du, Bo-Hua Liang, He Wang, Peng Xu, Ziren Luo, and Yueliang Wu. Advancing space-based gravitational wave astronomy: Rapid detection and parameter estimation using normalizing flows. 2023.
- [33] Maximilian Dax, Jonas Wildberger, Simon Buchholz, Stephen R. Green, Jakob H. Macke, and Bernhard Scholkopf. Flow matching for scalable simulation-based inference. *ArXiv*, abs/2305.17161, 2023.
- [34] Michael S Albergo, Nicholas M. Boffi, and Eric Vanden-Eijnden. Stochastic interpolants: A unifying framework for flows and diffusions. *ArXiv*, abs/2303.08797, 2023.
- [35] Alexander Tong, Kilian Fatras, Nikolay Malkin, Guillaume Hugué, Yanlei Zhang, Jarrid Rector-Brooks, Guy Wolf, and Yoshua Bengio. Improving and generalizing flow-based generative models with minibatch optimal transport, 2024.
- [36] Wen-Hong Ruan, He Wang, Chang Liu, and Zong-Kuan Guo. Rapid search for massive black hole binary coalescences using deep learning. *Physics Letters B*, 841:137904, 2023.
- [37] Sylvain Marsat and John G. Baker. Fourier-domain modulations and delays of gravitational-wave signals, 6 2018.
- [38] Geraint Pratten, Antoine Klein, Christopher J. Moore, Hannah Middleton, Nathan Steinle, Patricia Schmidt, and Alberto Vecchio. Lisa science performance in observations of short-lived signals from massive black hole binary coalescences. *Phys. Rev. D*, 107:123026, Jun 2023.
- [39] Ziren Luo, ZongKuan Guo, Gang Jin, Yueliang Wu, and Wenrui Hu. A brief analysis to taiji: Science and technology. *Results in Physics*, 16:102918, 2020.
- [40] Michele Vallisneri, Jeff Crowder, and Massimo Tinto. Sensitivity and parameter-estimation precision for alternate lisa configurations. *Classical and Quantum Gravity*, 25(6):065005, mar 2008.
- [41] Gang Wang, Wei-Tou Ni, Wen-Biao Han, Shu-Cheng Yang, and Xing-Yu Zhong. Numerical simulation of sky localization for LISA-TAIJI joint observation. *Phys. Rev. D*, 102(2):024089, 2020.
- [42] Gang Wang and Wei-Tou Ni. Revisiting time delay interferometry for unequal-arm LISA and TAIJI. *Phys. Scripta*, 98(7):075005, 2023.
- [43] Neil J. Cornish and Tyson B. Littenberg. Tests of bayesian model selection techniques for gravitational wave astronomy. *Phys. Rev. D*, 76:083006, Oct 2007.
- [44] Gang Wang, Zhen Yan, Bin Hu, and Wei-Tou Ni. Investigating galactic double white dwarfs for the sub-mHz gravitational wave mission ASTROD-GW. *Phys. Rev. D*, 107(12):124022, 2023.
- [45] Valeriya Korol, Elena M Rossi, and Enrico Barausse. A multimessenger study of the Milky Way’s stellar disc and bulge with LISA, Gaia, and LSST. *Monthly Notices of the Royal Astronomical Society*, 483(4):5518–5533, 12 2018.
- [46] Chang Liu, Wen-Hong Ruan, and Zong-Kuan Guo. Confusion noise from galactic binaries for taiji. *Phys. Rev. D*, 107:064021, Mar 2023.
- [47] Xue-Hao Zhang, Shao-Dong Zhao, Soumya D. Mohanty, and Yu-Xiao Liu. Resolving Galactic binaries using a network of space-borne gravitational wave detectors. *Phys. Rev. D*, 106(10):102004, 2022.
- [48] M. I. Jordan and T. M. Mitchell. Machine learning: Trends, perspectives, and prospects. *Science*, 349(6245):255–260, 2015.
- [49] Elena Cuoco, Jade Powell, Marco Cavaglia, Kendall Ackley, Michał Bejger, Chayan Chatterjee, Michael Coughlin, Scott Coughlin, Paul Easter, Reed Essick, Hunter Gabbard, Timothy

- Gebhard, Shaon Ghosh, Leïla Haegel, Alberto Iess, David Keitel, Zsuzsa Márka, Szabolcs Márka, Filip Morawski, Tri Nguyen, Rich Ormiston, Michael Pürrer, Massimiliano Razzano, Kai Staats, Gabriele Vajente, and Daniel Williams. Enhancing gravitational-wave science with machine learning. *Machine Learning: Science and Technology*, 2(1):011002, dec 2020.
- [50] Hunter Gabbard, Chris Messenger, Ik Siong Heng, Francesco Tonolini, and Roderick Murray-Smith. Bayesian parameter estimation using conditional variational autoencoders for gravitational-wave astronomy. *Nature Physics*, 18(1):112–117, 2022.
- [51] Chayan Chatterjee, Linqing Wen, Kevin Vinsen, Manoj Kovalam, and Amitava Datta. Using deep learning to localize gravitational wave sources. *Phys. Rev. D*, 100:103025, Nov 2019.
- [52] Stephen R. Green, Christine Simpson, and Jonathan Gair. Gravitational-wave parameter estimation with autoregressive neural network flows. *Phys. Rev. D*, 102:104057, Nov 2020.
- [53] Stephen R Green and Jonathan Gair. Complete parameter inference for gw150914 using deep learning. *Machine Learning: Science and Technology*, 2(3):03LT01, jun 2021.
- [54] Arnaud Delaunoy, Antoine Wehenkel, Tanja Hinderer, Samaya Nissanke, Christoph Weniger, Andrew R Williamson, and Gilles Louppe. Lightning-fast gravitational wave parameter inference through neural amortization, 2020.
- [55] Plamen G. Krastev, Kiranjyot Gill, V. Ashley Villar, and Edo Berger. Detection and parameter estimation of gravitational waves from binary neutron-star mergers in real ligo data using deep learning. *Physics Letters B*, 815:136161, 2021.
- [56] Hongyu Shen, E A Huerta, Eamonn O’Shea, Prayush Kumar, and Zhizhen Zhao. Statistically-informed deep learning for gravitational wave parameter estimation. *Machine Learning: Science and Technology*, 3(1):015007, nov 2021.
- [57] Maximilian Dax, Stephen R. Green, Jonathan Gair, Jakob H. Macke, Alessandra Buonanno, and Bernhard Schölkopf. Real-time gravitational wave science with neural posterior estimation. *Phys. Rev. Lett.*, 127:241103, Dec 2021.
- [58] Maximilian Dax, Stephen R. Green, Jonathan Gair, Michael Pürrer, Jonas Wildberger, Jakob H. Macke, Alessandra Buonanno, and Bernhard Schölkopf. Neural importance sampling for rapid and reliable gravitational-wave inference. *Phys. Rev. Lett.*, 130:171403, Apr 2023.
- [59] Yaron Lipman, Ricky TQ Chen, Heli Ben-Hamu, Maximilian Nickel, and Matt Le. Flow matching for generative modeling. *arXiv preprint arXiv:2210.02747*, 2022.
- [60] Maximilian Dax, Stephen R. Green, Jonathan Gair, Jakob H. Macke, Alessandra Buonanno, and Bernhard Schölkopf. Real-time gravitational wave science with neural posterior estimation. *Phys. Rev. Lett.*, 127:241103, Dec 2021.
- [61] Yann N. Dauphin, Angela Fan, Michael Auli, and David Grangier. Language Modeling with Gated Convolutional Networks. *arXiv e-prints*, page arXiv:1612.08083, December 2016.
- [62] Maximilian Dax, Stephen R. Green, Jonathan Gair, Michael Deistler, Bernhard Schölkopf, and Jakob H. Macke. Group equivariant neural posterior estimation. 11 2021.
- [63] Michele Vallisneri and Chad R. Galley. Non-sky-averaged sensitivity curves for space-based gravitational-wave observatories. *Class. Quant. Grav.*, 29:124015, 2012.
- [64] John Veitch and Alberto Vecchio. Bayesian coherent analysis of in-spiral gravitational wave signals with a detector network. *Physical Review D*, 81(6):062003, 2010.
- [65] John Skilling. Nested sampling for general bayesian computation. 2006.
- [66] Gregory Ashton, Moritz Hübner, Paul D Lasky, Colm Talbot, Kendall Ackley, Sylvia Biscoveanu, Qi Chu, Atul Divakarla, Paul J Easter, Boris Goncharov, et al. Bilby: A user-friendly bayesian inference library for gravitational-wave astronomy. *The Astrophysical Journal Supplement Series*, 241(2):27, 2019.